Solution effect on improved structural compatibility of NiTi-based alloys by systematic first-principles calculations

Lee, Joohwi; Ikeda, Yuji; Tanaka, Isao

Journal of Applied Physics ARTICLE scitation.org/journal/jap

Solution effect on improved structural compatibility of NiTi-based alloys by systematic first-principles calculations

Cite as: J. Appl. Phys. **125**, 055106 (2019); doi: 10.1063/1.5051630
Submitted: 10 August 2018 · Accepted: 15 January 2019 ·
Published Online: 4 February 2019

Joohwi Lee,[1,a,b] Yuji Ikeda,[1] and Isao Tanaka[1,2,3,4]

AFFILIATIONS

[1]Department of Materials Science and Engineering, Kyoto University, Kyoto 606-8501, Japan
[2]Elements Strategy Initiative for Structure Materials (ESISM), Kyoto University, Kyoto 606-8501, Japan
[3]Center for Materials Research by Information Integration, National Institute for Materials Science (NIMS), Tsukuba, Ibaraki 305-0047, Japan
[4]Nanostructures Research Laboratory, Japan Fine Ceramics Center, Nagoya, Aichi 456-8587, Japan

[a)]**Electronic mail:** lee.joohwi@gmail.com
[b)]**Present address:** Toyota Central R&D Laboratories, Inc., Nagakute, Aichi 480-1192, Japan.

ABSTRACT

The functional stability of a shape memory alloy (SMA) may be related to its structural compatibility between the parent-phase and the martensitic-phase structures. In this study, we perform systematic first-principles calculations for 276 Ni–Ti-based ternary alloys to investigate their energetic stability as well as their structural compatibility between the parent- and the martensitic-phase structures. We analyze in detail the dependences of the energetics and structural properties on the additional element X, on X concentration, and on the replaced chemical element. Some X are found to energetically stabilize the B19 structures more than the B19′ structures at X concentrations above 6.25 at. %. It is also found that the B19–B2 martensitic transformation shows better structural compatibility than the B19′–B2 transformation for most of the investigated ternary Ni–Ti–X alloys. These alloys also tend to have better structural compatibility than binary equiatomic NiTi. Moreover, we screen the investigated alloys on the basis of their energetic stability and structural compatibility, and we identify 26 Ni–Ti–X alloys as possible SMAs with good functional stability. In this study, we reveal a strong potential of the computational design for improving the functional stability of Ni–Ti SMAs by alloying additional elements.

I. INTRODUCTION

NiTi (also called nitinol) with a near-stoichiometric (equiatomic) composition ratio is one of the widely used shape memory alloys (SMAs)[1] and has many advantages such as good pseudoelasticity and phase stability.[2] Despite these advantages, the binary equiatomic NiTi still suffers from its poor functional stability; it shows a large thermal hysteresis as 50–60 K[3,4] and a severe functional fatigue behavior measured by the shift of the transformation temperature by 30 K after only 20 cycles.[5]

The functional stability of SMAs may be related to the structural compatibility between the parent-phase and the martensitic-phase structures of the alloys. James and Hane have shown that the parent-phase and the martensitic-phase structures can create a distortionless interface when the second largest eigenvalue λ_2 of the transformation stretch tensor **U** between two structures is equal to one.[6] According to this model, the poor functional stability of the binary equiatomic NiTi, which has the B19′ martensitic structure, can be ascribed to the deviation of $|\lambda_2 - 1|$ from zero reported as ~0.03 in experiments[7,8] and ~0.03–0.06 in computational results[9–12] (see Table I). To improve the functional stability of NiTi-based SMAs, it may be an effective strategy to make $|\lambda_2 - 1|$ close to zero.

TABLE I. Crystal structures with various phases of the binary equiatomic NiTi.

Phase (space group)	Method[a]	Ref.	a_1 (Å)	a_2 (Å)	a_3 (Å)	γ (°)	Volume (Å^3/atom)	det(U) − 1	$\lambda_2 - 1$	$E - E^{B2}$ (eV/atom)
B2 (*Pm*–3*m*)	Theory	This study	4.246	3.003	4.246	90.0	13.54			
	Theory[b,c,d]	9	4.255	3.009	4.255	90.0	13.62			
	Theory	10	4.258	3.011	4.258	90.0	13.65			
	Theory[b,e]	11	4.262	3.014	4.262	90.0	13.69			
	Theory[e]	11	4.255	3.009	4.255	90.0	13.62			
	Theory	12	4.253	3.007	4.253	90.0	13.60			
	Theory[b]	13	4.252	3.007	4.252	90.0	13.59			
	Theory[f]	17	4.270	3.019	4.270	90.0	13.76			
	Theory[b,d]	18	4.254	3.008	4.254	90.0	13.61			
	Theory[b]	26	4.260	3.012	4.260	90.0	13.67			
	Experiment	7	4.264	3.015	4.264	90.0	13.70			
	Experiment	55	4.266	3.016	4.266	90.0	13.72			
B19 (*Pmma*)	Theory	This study	4.631	2.731	4.249	90.0	13.44	−0.007	0.001	−0.033
	Theory[b,c,d]	9	4.631	2.776	4.221	90.0	13.57	−0.004	−0.008	−0.030
	Theory	10	4.707	2.810	4.189	90.0	13.85	0.015	−0.016	−0.029
	Theory[b,e]	11	4.602	2.840	4.120	90.0	13.46	−0.016	−0.033	−0.027
	Theory[e]	11	4.597	2.850	4.167	90.0	13.65	0.002	−0.021	−0.026
	Theory[b]	13	4.603	2.828	4.181	90.0	13.61	0.001	−0.017	−0.027
	Theory[f]	17	4.633	2.863	4.180	90.0	13.86	0.007	−0.021	−0.041
	Theory[b,d]	18	4.585	2.895	4.118	90.0	13.67	0.004	−0.032	−0.030
	Theory[b]	26	4.613	2.798	4.208	90.0	13.58	−0.006	−0.013	−0.029
B19′ and B19′′ ($P2_1/m$)	Theory	This study	4.767	2.916	4.032	102.2	13.70	0.012	−0.051	−0.043
	Theory	10	4.672	2.847	4.116	97.8	13.56	−0.006	−0.033	−0.039
	Theory[e]	11	4.678	2.933	4.108	98.3	13.94	0.019	−0.036	−0.041
	Theory[b,e]	11	4.801	2.923	4.042	102.4	13.88	0.014	−0.052	−0.044
	Theory[e]	11	4.819	2.926	4.034	103.2	13.84	0.017	−0.052	−0.047
	Theory	12	4.780	2.917	4.047	100.0	13.89	0.022	−0.048	−0.042
	Theory[b]	26	4.769	2.945	4.034	101.8	13.87	0.015	−0.053	−0.043
	Experiment	7	4.622	2.889	4.120	96.8	13.66	−0.003	−0.034	
	Experiment	8[g]	4.646	2.898	4.108	97.8	13.70	0.000	−0.037	
	Experiment	55	4.657	2.909	4.114	97.9	13.80	0.006	−0.036	
B33 (*Cmcm*)	Theory	This study	4.901	2.916	4.015	107.3	13.72	0.013	−0.054	−0.043[h]
	Theory[b,c,d]	9	4.936	2.940	3.997	107.0	13.87	0.018	−0.061	−0.050
	Theory[b,e]	11	4.923	2.928	4.017	106.6	13.87	0.014	−0.057	−0.046
	Theory[e]	11	4.925	2.926	4.012	106.5	13.86	0.018	−0.054	−0.049
	Theory	12	4.927	2.914	4.021	107.3	13.78	0.013	−0.055	−0.042[h]
	Theory[b]	13	4.925	2.929	4.015	107.3	13.82	0.017	−0.056	−0.042
	Theory[f]	17	4.928	2.933	4.025	107.0	13.91	0.003	−0.057	−0.060
	Theory[b,d]	18	4.951	2.953	3.993	108.5	13.84	0.017	−0.061	−0.050
	Theory[b]	26	4.926	2.932	4.012	107.3	13.83	0.012	−0.058	−0.044

[a]Theoretical results are obtained using the PAW method[31,32] in combination with the Perdew–Burke–Ernzerhof form[35] of the GGA and with including the 3p-orbital electrons of Ti in the core, unless separately footnoted.
[b]3p-orbital electrons of Ti are included in the valence.
[c]Vanderbilt ultrasoft pseudopotential.[56]
[d]Perdew-Wang form.[58]
[e]Gaussian basis function with double zeta plus polarization.
[f]Full-potential linearized augmented plane-wave (FLAPW) method.[57]
[g]Lattice parameter of the B2 parent-phase structure for calculating λ_2 is extracted from Ref. 7.
[h]Energy of the B33 structure is slightly (<0.001 eV) lower than that of the B19′ structure.

The structural property of alloys can be modified by adding other chemical elements. Several experiments have shown that the λ_2 of $Ni_{50-x}Ti_{50}X_x$ alloys can be tuned to be close to one by replacing Ni with various chemical elements X. Zhang *et al.* have shown that the λ_2 of $Ni_{50-x}Ti_{50}X_x$ (X = Cu, Pd, Pt, or Au) can be adjusted to one, and the thermal hysteresis of these alloys markedly decreases to be lower than 20 K.[3] Zarnetta *et al.* have shown that the functional fatigue of Ni–Ti–Cu–Pd alloys can be improved to be 0.1 K after 80 cycles by adjusting λ_2 to one by changing their composition ratio.[5]

We expect that other X may also improve the structural compatibility of Ni–Ti–X alloys. To investigate various possible Ni–Ti–X alloys systematically, first-principles calculations are useful. Many computational studies have already been performed for specific Ni–Ti(–X) alloys, such as comparisons of various crystal and electronic structures,[9–15] the

transformation path between the parent-phase and martensitic-phase structures,[10,16–18] and the energetic stability changes by point defects, for example, vacancies, antisites, and interstitial atoms.[13,19–22] The site preferences of tens of different alloying elements in NiTi in the B2 parent-phase structure were also investigated.[23] However, the impact of alloying on the structural compatibility between the parent-phase and the martensitic-phase structures of the NiTi-based alloys has not been investigated in detail by first-principles calculations, to the best of our knowledge.

In this study, we perform systematic first-principles calculations to investigate the energetic stability and the structural compatibility between the parent-phase and the martensitic-phase structures of the Ni–Ti–X ternary alloys for various alloying elements X, including those not well investigated in experiments. We analyze the dependences of these properties on the type of X, on its concentration, and on the replaced site. The site preference of X was also analyzed both in the parent-phase and martensitic-phase structures. We finally screened the investigated ternary Ni–Ti–X alloys on the basis of their energetic stability and structural compatibility and found that 26 Ni–Ti–X alloys may have good functional stability as SMAs.

II. COMPUTATIONAL DETAILS

A. Crystal structures

Figure 1 shows the computational unit cells of the B2, B19, and B19′ crystal structures of the binary equiatomic NiTi. The B2 structure was considered to be the parent phase, and the B19 (2H in the Ramsdell notation[24]) and B19′ structures were considered to be the possible martensitic phases. The computational unit cell of each crystal structure contains four atoms. Note that while the B2 structure has the cubic crystallographic symmetry, in this study, we used the tetragonal computational unit cell to make it similar to the unit cells of the B19 and B19′ structures. This enables us to consider a consistent atomic configuration among the B2, B19, and B19′ structures, which are related to each other through martensitic transformations.

The models of binary nonstoichiometric Ni–Ti alloys and ternary Ni–Ti–X alloys with the alloying element X were constructed on supercells of the above unit cells for the binary equiatomic NiTi. The binary nonstoichiometric alloys were modeled by substituting one Ni atom for a Ti atom (a Ni antisite, denoted as Ni_{Ti}) or by substituting one Ti atom for a Ni atom (a Ti antisite, denoted as Ti_{Ni}). The ternary alloys were modeled by substituting one X atom for a Ni atom (X_{Ni}) or a Ti atom (X_{Ti}). We used the supercells of $2\times4\times2$, $1\times2\times2$, and $1\times2\times1$ to describe the point-defect concentrations of 1/64 (1.5625 at. %), 1/16 (6.25 at. %), and 1/8 (12.5 at. %), respectively. Note that the B2 structure of the binary equiatomic NiTi is known to be dynamically unstable at 0 K,[11,14–16,25–30] which indicates that we also need to carefully model the B2 structure of the binary nonstoichiometric Ni–Ti and the ternary Ni–Ti–X alloys not to break their expected atomic configurations. The current one-atom-replaced supercell models still have crystallographically high symmetries, and hence we can keep the expected atomic configurations of the B2 structure because of the symmetry constraint during the structural optimization. We chose 46 metallic elements between Li and Bi in the periodic table as X. In total, we investigated 276 Ni–Ti–X ternary alloys with different types of X, different concentrations of X, or different replaced chemical elements (Ni or Ti).

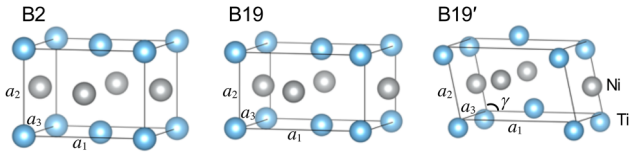

FIG. 1. Computational unit cells of the B2, B19, and B19′ crystal structures of the binary equiatomic NiTi.

B. First-principles calculations

First-principles calculations were performed using the projector augmented wave (PAW) method[31,32] implemented in the Vienna *ab initio* Simulation Package (VASP)[33,34] within the framework of the generalized gradient approximation (GGA) of the Perdew–Burke–Ernzerhof form.[35] The cutoff energy was set to 400 eV. The Methfessel–Paxton scheme[36] with a bit large smearing width of 0.4 eV was employed for Brillouin zone integration to achieve the convergence for all the calculations. The B2 structure was sequentially optimized by first relaxing its volume while maintaining the lattice shape, and then relaxing the internal atomic coordinates. For comparison, we also constructed a cubic supercell model of the B2 structure for each composition, where the alloying element X was put on the center or both on the center and the corner of the simulation cell to keep the cubic symmetry, and optimized the cell volume and the internal atomic coordinates simultaneously. The lattice parameters obtained in this way were not largely different from those obtained from the tetragonal supercell models by the sequential optimization, as demonstrated by the average and the maximum differences of the lattice parameters of ~0.09% and ~0.74%, respectively. The B19 and B19′ structures were optimized by relaxing their volumes, shapes, and internal coordinates simultaneously. For binary nonstoichiometric and ternary alloys, the structural optimizations were started from the optimized geometry for binary equiatomic NiTi. The relaxations were performed until the residual forces acting on atoms reach below 0.005 eV/Å. The s- and d-electrons were used as valence electrons for Ni and Ti (For the effect of different valence electrons, see Refs. 11 and 14 and the supplementary material). The $\boldsymbol{k}$-space meshes of the Γ-centered $16\times24\times16$/unit-cell were employed for the binary Ni–Ti and the ternary Ni–Ti–X alloys. Both the nonmagnetic (NM) and ferromagnetic (FM) states were first calculated for each model, and the lower-energy state was investigated in the following analysis.

C. Energetics

The energetics of the investigated systems were discussed on the basis of their formation energies. In this study, the formation energies of a phase α, ΔE_f^α, were computed by setting the mixture of single metals as references. Two situations were considered for the alloying of an additional element X in the Ni–Ti alloy, as shown in Fig. 2(a); one is that X occupies a deficient-element site, and the other is that X occupies a rich-element site generating a rich-element antisite. We computed the formation energies of these two X-alloying situations and compared them to analyze the site preference of X. For the cases where X occupies a deficient-element site, we computed the formation energies [ΔE_f^α (with X_{Ni}) and ΔE_f^α (with X_{Ti}) for the Ni-deficient and Ti-deficient conditions, respectively, where the symbols in the parentheses indicate the existing point defects] straightforwardly. For the cases where X occupies a rich-element site, generating a rich-element antisite, we computed the formation energies in an indirect manner under the assumption of negligible interaction between X and the antisite [Fig. 2(b)]. Specifically, the formation energies in this with-antisite situation were approximated as

$$\Delta E_f^\alpha(\text{with } X_{Ti} \text{ and } Ti_{Ni}) \approx \Delta E_f^\alpha(\text{with } X_{Ti}) + \Delta E_f^\alpha(\text{with } Ti_{Ni}) - \Delta E_f^\alpha(\text{perfect}) \quad (1)$$

and

$$\Delta E_f^\alpha(\text{with } X_{Ni} \text{ and } Ni_{Ti}) \approx \Delta E_f^\alpha(\text{with } X_{Ni}) + \Delta E_f^\alpha(\text{with } Ni_{Ti}) - \Delta E_f^\alpha(\text{perfect}), \quad (2)$$

for the Ni-deficient and Ti-deficient conditions, respectively. In this study, we analyzed the site preference of X in Ni–Ti in the B2, B19, and B19′ structures.

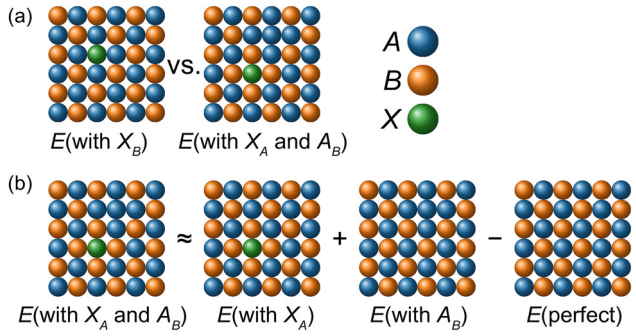

FIG. 2. Two-dimensional schematic representation of an ordered binary *AB* alloy including an alloying element *X*. Blue, orange, and green spheres denote the elements *A*, *B*, and *X*, respectively. (a) Comparison between cases where *X* is at the *B* site (X_B) and at the *A* site, creating the *A* antisite (X_A and A_B) under the *B*-deficient condition. (b) Assumption that no interaction exists between X_A and A_B under the *B*-deficient condition, which was employed to compute the energy of Ni–Ti–*X* alloys when *X* is at the Ni (Ti) site, creating the Ni (Ti) antisite under the condition of Ti (Ni) deficiency.

The energetic stabilities among the B2, B19, and B19′ structures were also analyzed by comparing their formation energies. In particular, it may be necessary for the martensitic-phase structure to have lower energy than the B2 structure at 0 K to guarantee the existence of martensitic transformation between the B2 parent-phase structure at high temperature and the B19 or B19′ martensitic-phase structure at low temperature.[25]

To ensure that the considered martensitic transformations occur in reality, it may also be better for the energetically favorable martensitic-phase structure between the B19 and B19′ structures to be energetically more stable than other possible states. It is well known that the convex-hull states of the binary Ni-Ti systems consist of NiTi, $NiTi_2$, and Ni_3Ti. Therefore, we compared the formation energy of the more stable martensitic-phase structure with that of a phase-separation state consisting of NiTi, $NiTi_2$, Ni_3Ti, and pure X. The Ni-replaced $Ni_{n-1}Ti_{n+1}$ and the Ti-replaced $Ni_{n+1}Ti_{n-1}$ binary nonstoichiometric alloys should satisfy

$$\Delta E_f^m(Ni_{n-1}Ti_{n+1}) - \Delta E_f(NiTi + NiTi_2) = \Delta E_f^m(Ni_{n-1}Ti_{n+1}) - \frac{1}{n}[(n-3)\Delta E_f^{B19'}(NiTi) + 3\Delta E_f(NiTi_2)] < 0 \quad (3)$$

and

$$\Delta E_f^m(Ni_{n+1}Ti_{n-1}) - \Delta E_f(NiTi + Ni_3Ti) = \Delta E_f^m(Ni_{n+1}Ti_{n-1}) - \frac{1}{n}[(n-2)\Delta E_f^{B19'}(NiTi) + 2\Delta E_f(Ni_3Ti)] < 0, \quad (4)$$

respectively. Similarly, the Ni-replaced $Ni_{n-1}Ti_nX$ and the Ti-replaced $Ni_nTi_{n-1}X$ ternary alloys should satisfy

$$\Delta E_f^m(Ni_{n-1}Ti_nX) - \Delta E_f(NiTi + NiTi_2 + X) = \Delta E_f^m(Ni_{n-1}Ti_nX) - \frac{1}{2n}[(2n-4)\Delta E_f^{B19'}(NiTi) + 3\Delta E_f(NiTi_2) + \Delta E_f(X)] < 0 \quad (5)$$

and

$$\Delta E_f^m(Ni_nTi_{n-1}X) - \Delta E_f(NiTi + Ni_3Ti + X) = \Delta E_f^m(Ni_nTi_{n-1}X) - \frac{1}{2n}[(2n-3)\Delta E_f^{B19'}(NiTi) + 2\Delta E_f(Ni_3Ti) + \Delta E_f(X)] < 0, \quad (6)$$

respectively.

D. Structural change between the parent-phase and the martensitic-phase structures

The transformation stretch tensor **U**, which is a positive-definite symmetric matrix, provides us two properties related to structural change between the parent-phase and martensitic-phase structures, namely, the second largest eigenvalues (λ_2) of **U** and the determinant of **U** [det(**U**)]. λ_2 denotes the structural compatibility between the parent-phase and martensitic-phase structures,[6] and det(**U**) denotes the

ratio of the volumes of the martensitic-phase and parent-phase structures. Experimental reports have revealed that λ_2 shows a strong correlation with the functional stability of Ni–Ti-based ternary alloys.[3,4]

We can obtain **U** from lattice vectors of the parent-phase and the martensitic-phase structures in the following way. First, suppose that three linearly independent lattice vectors of the parent-phase structure, $\mathbf{v}^p_1$, $\mathbf{v}^p_2$, and $\mathbf{v}^p_3$, are transformed into the lattice vectors of the martensitic-phase structure, $\mathbf{v}^m_1$, $\mathbf{v}^m_2$, and $\mathbf{v}^m_3$, respectively, after the martensitic transformation. Then, the deformation gradient **F**[6] is calculated as

$$\mathbf{F} = \mathbf{V}^m(\mathbf{V}^p)^{-1}, \tag{7}$$

where $\mathbf{V}^p = (\mathbf{v}^p_1 \cdot \mathbf{v}^p_2 \cdot \mathbf{v}^p_3)$ and $\mathbf{V}^m = (\mathbf{v}^m_1 \cdot \mathbf{v}^m_2 \cdot \mathbf{v}^m_3)$ are the 3×3 matrices defined by the lattice vectors in column form. Finally, **U** is determined by polar decomposition of **F** as

$$\mathbf{F} = \mathbf{RU}, \tag{8}$$

where **R** is a rotation matrix.

III. RESULTS AND DISCUSSION

A. Binary equiatomic NiTi

Here, we analyze the structural properties of the binary equiatomic NiTi. Table I shows the structural and energetic properties of the B2, B19, B19′, and B33 structures of the binary equiatomic NiTi computed in this study. Experimental and other computational values in the literature are also shown for comparison. Here, among the many preceding computational results, we picked up the values obtained using GGA without any structural constraints during the structural optimization.

Although the monoclinic B19′ structure (space group $P2_1/m$) is known as the martensitic-phase structure of the binary equiatomic NiTi in experiments, first-principles calculations have indicated the body-centered orthorhombic B33 structure (space-group type of *Cmcm*) to be the ground state.[9] Many subsequent computational studies,[11,12,14,17,18] including our present calculation (see additional information in the supplementary material), also reveal that the B33 structure is energetically the most stable. We do not focus on the B33 structure hereafter for the following reasons. Firstly, the B33 structure has not been observed in experiments. Secondly, recent first-principles molecular-dynamics (MD) simulations revealed that the B33 structure is dynamically unstable around room temperature.[14] Finally, even if the B33 structure is obtained in experiments, it cannot have the shape memory effect because the B33–B2 transformation is not uniquely determined due to the high symmetry of the B33 structure.[9] We also note that the B33–B2 transformation shows poor structural compatibility as $|\lambda_2 - 1| > 0.05$, which is expected to result in poor functional stability.

Although the B19′ structure is observed in experiments with the monoclinic angle γ of approximately 97°,[7,8] its dynamical stability has been controversial among the reports of first-principles calculations. Huang *et al.*,[9] Holec *et al.*,[12] and Mizuno *et al.*[13] claimed that the B19′ structure is dynamically unstable at zero pressure, and Wagner and Windl[18] claimed that the B19′ structure with γ of approximately 97° can be obtained at a higher pressure of about 1 GPa. Vishnu and Strachan[11] claimed that the dynamical stability of the B19′ structure depends on whether we include the 3*p* electrons of Ti as valences in the calculation. Vishnu and Strachan[11] and Holec *et al.*[12] obtained the dynamically stable monoclinic structure but with γ more than 100°; it was referred to as the B19″ structure and was distinguished from the B19′ structure. Haskins *et al.*[14] claimed that the coexistence of the B19′ and B19″ structures is merely an artifact of low computational accuracy. Recent MD studies demonstrated that γ decreases with increasing temperature,[14,26] which may explain the overestimation of γ in the first-principles calculations at 0 K from γ in experiments observed at room temperature. In this study, we obtained the monoclinic structure with γ of ~102° after the structural relaxation.

The $\lambda_2 - 1$ values of the B19–B2 and the B19′–B2 structure transformations are largely different although the B19 and B19′ martensitic-phase structures are similar in volume to the B2 structure. In the present calculation, $|\lambda_2 - 1|$ of the B19–B2 transformation is only 0.001, while $|\lambda_2 - 1|$ of the B19′–B2 transformation is approximately 0.05. The experimental values of the B19′–B2 transformation also show $|\lambda_2 - 1|$ of approximately 0.03,[7,8] which is closer to our computational value for the B19′–B2 transformation than that for the B19–B2 transformation. This result indicates that the B19–B2 transformation has much better structural compatibility than the B19′–B2 transformation. Actually, as detailed in Secs. III B–III E, most of the investigated Ni–Ti-based alloys also show better structural compatibility for the B19–B2 transformation than for the B19′–B2 transformation. For the binary equiatomic NiTi, the B19′ structure is 0.01 eV/atom lower in energy than the B19 structure. We expect that the functional stability of SMAs can be improved when the B19 structure is energetically more stable than the B19′ structure in the martensitic phase.

B. Binary nonstoichiometric Ni–Ti alloys

Table II summarizes the computed structural and energetic properties of binary nonstoichiometric Ni–Ti alloys, which were modeled by replacing one Ni or Ti atom with the other in the supercells of the binary equiatomic NiTi. When 1.5625 at. % Ni or Ti is replaced with the other, the B19′ structure is still energetically more stable than the B19 structure, like the binary equiatomic NiTi. The energy difference between the B2 and B19′ structures decreases at these composition ratios. This is consistent with the computational result for the nonstoichiometric Ni–Ti alloys with the deviation of the composition ratio up to ~1.6 at. %.[22] When 6.25 at. % or more Ni or Ti are replaced with the other, the B19 structure is energetically more stable than the B19′ structure, which is consistent with a finding in a previous first-principles study.[13] For $Ni_{62.5}Ti_{37.5}$, the B19′ structure was found to converge into the B19 structure after the structural optimization.

For most of the compositions, the B19 structure has smaller $|\lambda_2 - 1|$ than the B19′ structure, which means that

TABLE II. Structural properties and energetics of the binary nonstoichiometric Ni–Ti alloys.

Alloy	Structure	γ (°)	$\lambda_2 - 1$	det(U) − 1	$E - E^{B2}$ (eV/atom)	ΔE_f(Ni–Ti) − ΔE_f(NiTi + $NiTi_2$) (eV/atom)	ΔE_f(Ni–Ti) − ΔE_f(NiTi + Ni_3Ti) (eV/atom)
$Ni_{48.4375}Ti_{51.5625}$ ($Ni_{31}Ti_{33}$)	B2	90.00			0.000	0.048	NA[a]
	B19	90.00	−0.008	−0.003	−0.027	0.021	NA
	B19′	99.63	−0.042	0.010	−0.035	0.013	NA
$Ni_{43.75}Ti_{56.25}$ (Ni_7Ti_9)	B2	90.00			0.000	0.062	NA
	B19	90.00	−0.009	0.002	−0.011	0.051	NA
	B19′	97.79	−0.004	0.005	−0.010	0.052	NA
$Ni_{37.5}Ti_{62.5}$ (Ni_3Ti_5)	B2	90.00			0.000	0.104	NA
	B19	90.00	−0.010	0.002	−0.002	0.077	NA
	B19′	101.29	−0.022	0.019	0.023	0.102	NA
$Ni_{51.5625}Ti_{48.4375}$ ($Ni_{33}Ti_{31}$)	B2	90.00			0.000	NA	0.032
	B19	90.00	−0.003	−0.006	−0.017	NA	0.015
	B19′	97.70	−0.026	0.002	−0.020	NA	0.012
$Ni_{56.25}Ti_{43.75}$ (Ni_9Ti_7)	B2	90.00			0.000	NA	0.068
	B19	90.00	0.020	−0.013	−0.030	NA	0.038
	B19′	105.45	−0.026	0.004	0.001	NA	0.069
$Ni_{62.5}Ti_{37.5}$ (Ni_5Ti_3)	B2	90.00			0.000	NA	0.124
	B19	90.00	0.016	−0.012	−0.082	NA	0.042
	B19′[b]	90.19	0.016	−0.011	−0.082	NA	0.042

[a]Not applicable.
[b]The B19′ structure is found to converge into the B19 structure after structural optimization.

the B19 structure has better structural compatibility with the parent-phase structure than the B19′ structure does. However, it is also found that the B19 and B19′ structures of all these nonstoichiometric binary alloys are energetically less stable than the phase-separation state, namely, NiTi + $NiTi_2$ or NiTi + Ni_3Ti. These phase separations are therefore expected to occur. The same trend is found also for the deviation of the composition ratio up to ~1.6 at. % by first-principles calculations.[22] Experiments have actually revealed the precipitations of Ni_3Ti and $NiTi_2$ at the Ni-rich and Ti-rich composition ratios, respectively.[2,37] Other precipitations such as Ni_4Ti_3 and Ni_3Ti_2 were also experimentally found at the Ni-rich region depending on aging conditions,[2] which implies that other types of phase separations may also occur. These results indicate the difficulty of improving the structural compatibility between the parent-phase and martensitic-phase structures as well as the functional stability of the Ni–Ti alloys as SMAs merely by adjusting their composition ratios.

C. Site preference of *X* in Ni–Ti–*X* alloys

Next, we consider adding the third chemical element X into the NiTi. We discuss the site preference of X (Sec. III C), energetic stabilities of the parent-phase and martensitic-phase structures (Sec. III D), and structural compatibility between the parent-phase and martensitic-phase structures (Sec. III E) for the 276 investigated Ni–Ti–X alloys. These properties of the Ni–Ti–X alloys are summarized in Sec. III F.

In previous computational studies, the site preference of X in Ni–Ti–X alloys in the B2 parent-phase structure was investigated by comparing the energies between the cases of X occupying a deficient-element site [Fig. 2(a)] and a rich-element site with the creation of a rich-element antisite [Fig. 2(b)]. Bozzolo *et al.* used their developed semiempirical model and reported that Fe, Pt, Pd, Au, Al, Cu, Zr, and Hf prefer direct substitution for the deficient site for the $Ni_{50-x}Ti_{50}X_x$ and $Ni_{50}Ti_{50-x}X_x$ alloys in the B2 structures.[38,39] In contrast, Singh *et al.* performed first-principles calculations for 34 types of X for the B2 structures of $Ni_{15}Ti_{16}X$ and $Ni_{16}Ti_{15}X$ alloys (3.125 at. % X) and found that the middle transition metals tend to occupy the Ni site, whereas the early and late transition metals tend to occupy the Ti site, regardless of the deficient element.[23] Manley *et al.* reported that the B2 structure of the $Ni_{50}Ti_{47}Fe_3$ alloy energetically prefers the substitution of Fe for Ni, creating a Ni antisite in their first-principles calculations, which is supported by Mössbauer spectroscopy and neutron diffraction.[20] These computational reports focused only on the B2 structure and/or a specific concentration of X. Therefore, the dependences of the site preference on the crystal structures and on the concentration of X are also worth investigating.

Figure 3 shows the site preference of X for the 276 investigated Ni–Ti–X alloys in the B2 parent-phase structure. Under the Ni-deficient condition [Fig. 3(a)], the elements in groups 5–10 mostly prefer to occupy the deficient Ni site, whereas the elements in groups 1–4 mostly prefer to occupy the rich Ti site, creating the Ti antisite. The elements in groups 11–15 show different site preferences from each other. Under the Ti-deficient condition [Fig. 3(b)], the elements in groups 1–5 and 10–15 mostly prefer to occupy the deficient Ti site, whereas the elements in groups 6–9 mostly prefer to occupy the rich Ni site, creating the Ni antisite.

The site preference of X is also found not to strongly depend on the X concentration. As the X concentration increases, the absolute values of E(with X_{Ni}) − E(with X_{Ti} and Ti_{Ni})

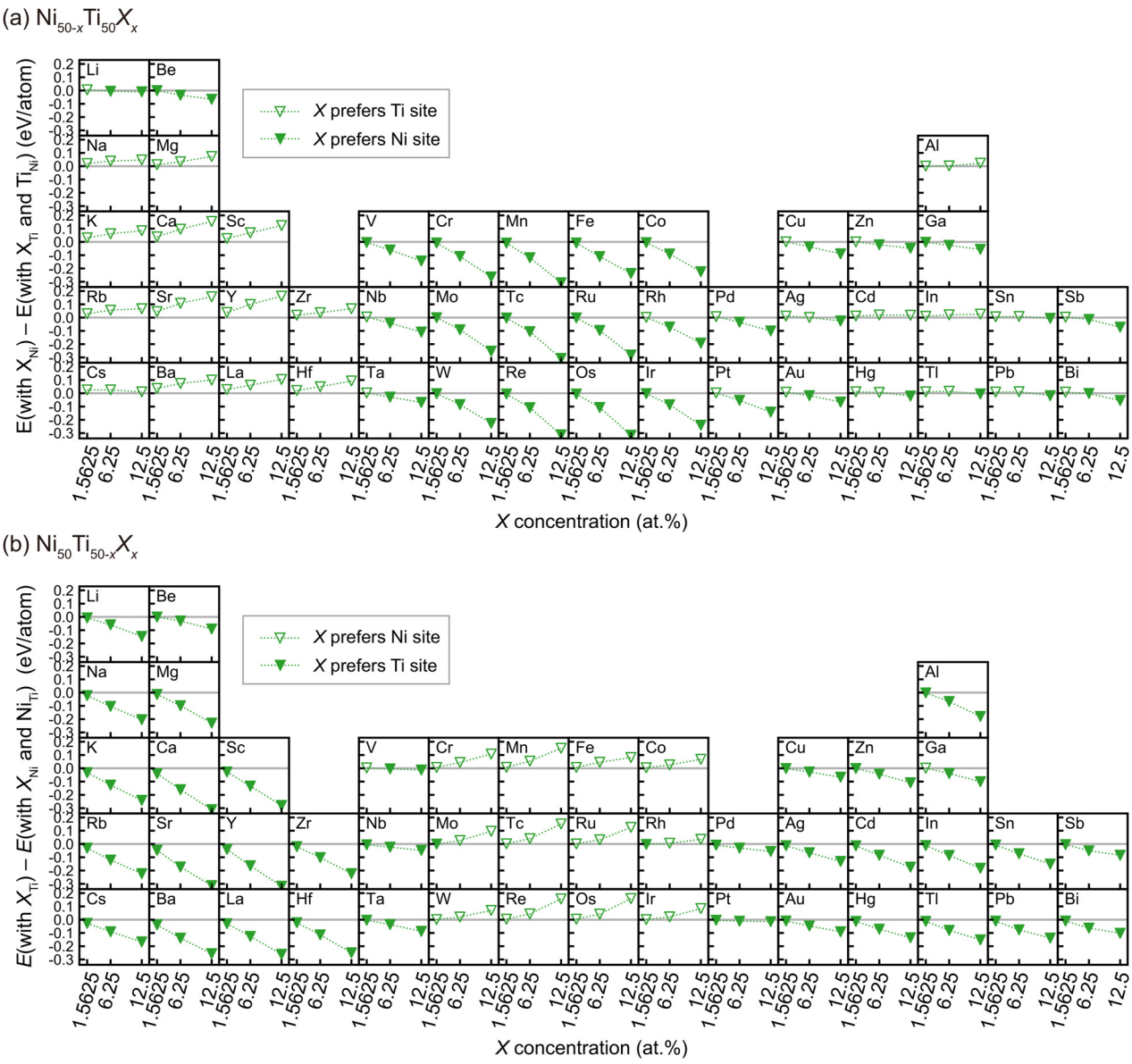

FIG. 3. Site preference of *X* in the B2 structures in the ternary (a) $Ni_{50-x}Ti_{50}X_x$ alloys (Ni-deficient condition) and (b) $Ni_{50}Ti_{50-x}X_x$ alloys (Ti-deficient condition). Filled symbols indicate that the substitution of *X* for the deficient-element site is energetically more favorable than the substitution of *X* for the rich-element site, creating the rich-element antisite. Dotted lines connecting the symbols are guides for the eyes.

and *E*(with X_{Ti}) – *E*(with X_{Ni} and Ni_{Ti}) under the Ni- and Ti-deficient conditions tend to increase, respectively.

Our results on the site preference of X mostly agree with those obtained previously by first-principles calculations and experiments. We find the tendency that middle transition metals prefer the Ni site, whereas the early and late transition metals prefer the Ti site. This tendency is the same as in the first-principles results obtained by Singh *et al.*,[23] who investigated 3.125 at. % X alloying in the B2 structure. The site preference of Fe for the Ni site under the Ti-deficient condition is consistent with the results obtained by Manley *et al.*[20] Only a few remarks for the comparison between our results and those reported previously are needed. In our results, some X such as Cu and Pd under the Ni-deficient condition have different site preferences when the concentrations of X are 1.5625 and 6.25 at. %; in these cases, we cannot straightforwardly compare our results with those in Ref. 23 in which X of 3.125 at. % was employed. Zr and Pt are found to prefer

the deficient Ti site under the Ti-deficient condition in our results, whereas in Ref. 23, it was reported that these chemical elements prefer the rich Ni site in the Ti-deficient condition. These differences might be ascribed to the different modeling for the B2 structure; we retained the cubic symmetry in the alloyed B2 structure, whereas such a symmetry constraint was not applied in Ref. 23. The B2 structure of the binary equiatomic NiTi is actually known to be dynamically unstable at 0 K,[11,14–16,25–30] and a small amount of alloying may not change this dynamical instability. The converged structures without any symmetry constraints may therefore be far away from the B2 structure for some Ni–Ti–X alloys.

Figure 4 shows the site preference of X for the 276 investigated Ni–Ti–X alloys in the B19 and B19′ martensitic-phase structures. The dependences of the site preference of X tend to be similar between the B2 parent-phase and martensitic-phase structures for many types of X. For some X, however, there are several differences from the results of the B2 structures. The elements in groups 11–15 prefer the deficient-element site in the martensitic-phase structures, whereas in the B2 structures, these chemical elements show different site preferences depending on the type of X. Moreover, for example, when Pt is 12.5 at. % alloyed, Pt prefers the deficient-element site in the B2 structure, while in the martensitic-phase structures, Pt prefers the Ni site regardless of the deficient element. In such cases, we need to carefully discuss which sites X occupies in reality; when the site preference of X is different between the B2 parent-phase and martensitic-phase structures, after the martensitic transformation, X still possibly occupies its preferred site before the transformation owing to the energy barrier for the atomic diffusion of X.

D. Energetic stability of Ni–Ti–*X* alloys in the parent-phase and martensitic-phase structures

Here, we discuss the energetic stability of Ni–Ti–X alloys in the parent-phase and martensitic-phase structures. Note that, hereafter, we only focus on the case where X occupies the deficient-element site for the sake of simplicity as well as for consistency with the discussion on the structural properties in Sec. III E.

Figure 5 shows the energies of the B19 and B19′ structures relative to those of the B2 structure for the 276 investigated Ni–Ti–X alloys. The energies of the martensitic-phase structures should be lower than that of the B2 parent-phase structure to enable the martensitic transformation.[25] Therefore, to consider the possibility for use as SMAs, the Ni–Ti–X alloys should satisfy the conditions $E^{B19'} - E^{B2} < 0$ or $E^{B19} - E^{B2} < 0$. An energy tolerance of 0.001 eV/atom was used to exclude the alloys in which the martensitic structures converged into the B2 structures. For 15 Ni–Ti–X alloys, both the B19 and the B19′ structures are energetically less stable than the B2 structure. These alloys consist of $Ni_{37.5}Ti_{50}X_{12.5}$ with X of the elements in groups 5–7, $Ni_{50}Ti_{37.5}X_{12.5}$ with X of Cd, Hg, Al, In, and Tl, and $Ni_{50}Ti_{43.75}Ag_{6.25}$. Shape memory effects may be lost in these 15 Ni–Ti–X alloys. For the other 261 Ni–Ti–X alloys, either or both of the B19 and the B19′ structures are energetically more stable than the B2 structure.

Figure 6 shows the energies of the B19′ structure relative to those of the B19 structure for the 276 investigated Ni–Ti–X alloys. Here, to compare the energies between the B19 and the B19′ structures, we employed the condition $E^{B19'} - E^{B19} < 0$ with an energy tolerance of 0.001 eV/atom to exclude the alloys in which the B19′ structure actually converged into the B19.

When 1.5625 at. % X is included, all of the B19′ structures of Ni–Ti–X alloys are energetically more stable than the B19 structure regardless of the substituted chemical element X and regardless of whether Ti or Ni is replaced with X. As detailed in Sec. III E, the B19′–B2 transformation tends to have less structural compatibility than the B19–B2 transformation. The result therefore indicates that the functional stability of Ni–Ti–X alloys as SMAs is not greatly improved from the binary equiatomic NiTi upon adding any of the investigated X at 1.5625 at. %.

When 6.25 at. % X is substituted, the B19 structures are energetically more favorable than the B19′ structures for some Ni–Ti–X alloys. When 6.25 at. % Ni is replaced by X, 13 out of the 46 $Ni_{43.75}Ti_{50}X_{6.25}$ alloys are energetically more stable in the B19 structure than in the B19′ structure. These X types consist only of some elements in groups 5–9 as well as K. In contrast, when 6.25 at. % Ti is replaced by X, 23 out of the 46 $Ni_{50}Ti_{43.75}X_{6.25}$ alloys are energetically more stable in the B19 structure than in the B19′ structure. These X types consist of most of the elements in groups 5–12 as well as some elements in groups 1–2, namely, Li, Na, K, and Be. When 12.5 at. % X is included, more types of X stabilize the B19 structure more than the B19′ structure. It is found that 38 $Ni_{37.5}Ti_{50}X_{12.5}$ and 25 $Ni_{50}Ti_{37.5}X_{12.5}$ alloys have the B19 structure that is energetically more stable than the B19′ structure. These X types are found in most of the groups in the periodic table.

Figure 7 shows the difference between the ΔE_f^m(Ni–Ti–X) of the investigated 276 Ni–Ti–X alloys and the ΔE_f of the phase-separation states at their corresponding composition ratios. Among them, only 91 Ni–Ti–X alloys have either or both of the martensitic-phase structures that are energetically more stable than the phase-separation states. For the $Ni_{50-x}Ti_{50}X_x$ alloys, some X in group 2 or groups 6–15 are found to stabilize the martensitic-phase structure more than the phase separation of NiTi + $NiTi_2$ + X. For the $Ni_{50}Ti_{50-x}X_x$ alloys, some X in groups 3–4, 8–11, or 13–15 are found to stabilize the martensitic-phase structure more than the phase separation of NiTi + Ni_3Ti + X. These alloys are likely to keep the ternary alloys without phase transition or phase separation. In contrast, the Ni–Ti–X alloys with much higher energy (approximately more than 0.1 eV/atom) than the phase-separation states, which are mainly found with X in groups 1 and 2, are probably difficult to form and cause a phase transition or a phase separation.

E. Structural compatibility of Ni–Ti–*X* alloys

Figure 8 shows the computed $\lambda_2 - 1$ of the 276 Ni–Ti–X alloys. The B19 structures of most (239 out of 276) of the

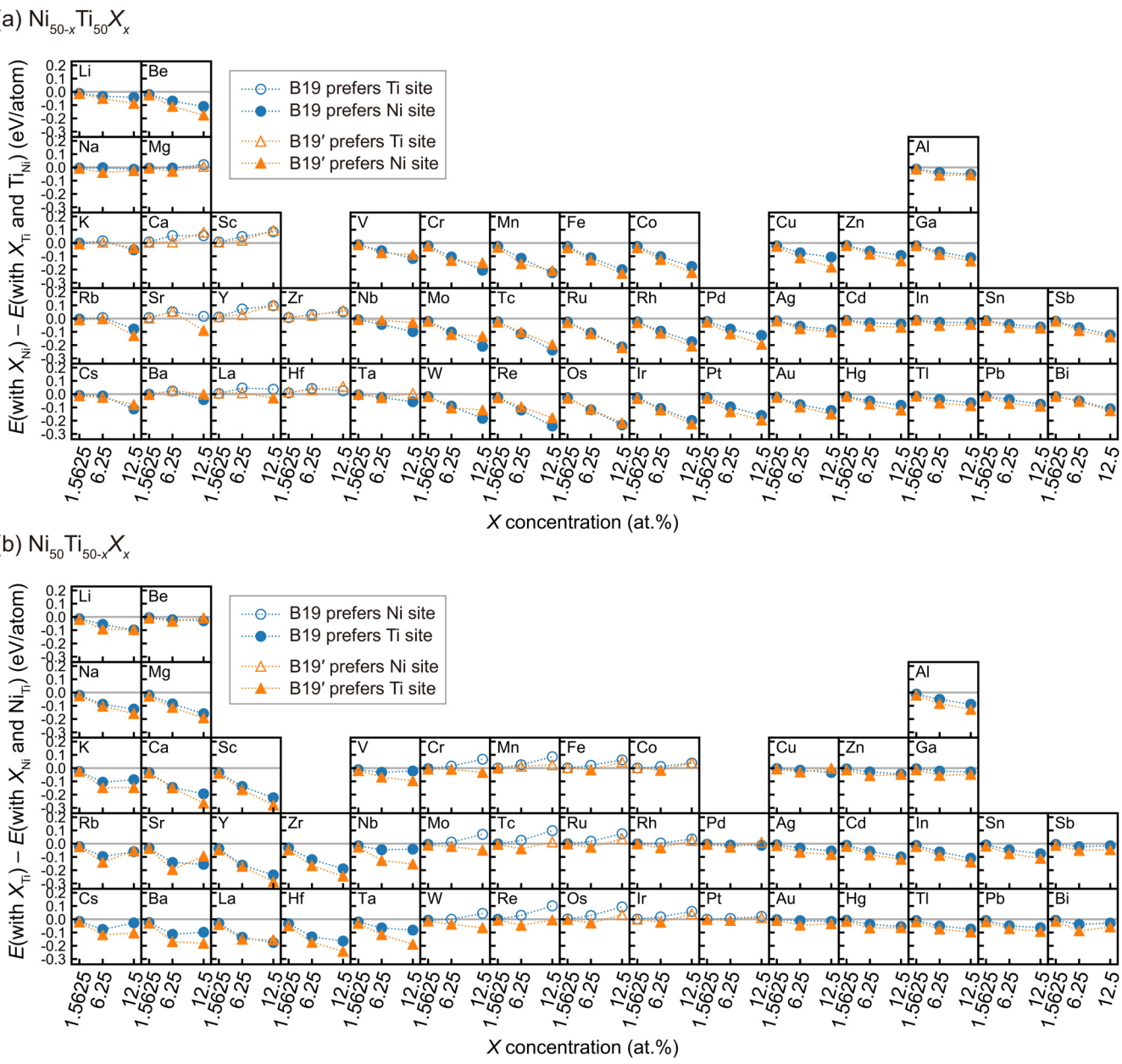

FIG. 4. Site preference of X in the B19 and B19′ structures in the ternary (a) $Ni_{50-x}Ti_{50}X_x$ alloys (Ni-deficient condition) and (b) $Ni_{50}Ti_{50-x}X_x$ alloys (Ti-deficient condition). Blue circles and orange triangles indicate the B19 and B19′ structures, respectively. Filled symbols indicate that the substitution of X for the deficient-element site is energetically more favorable than the substitution of X for the rich-element site, creating the rich-element antisite. Dotted lines connecting the symbols are guides for the eyes.

Ni–Ti–X alloys are found to have smaller $|\lambda_2 - 1|$ than the B19′ structures, regardless of the type of X, the X concentration, and the replaced site. This means that for most of the Ni–Ti–X alloys, the B19 structures have better structural compatibility than the B19′ structures. Note that several alloys do not follow this tendency; their B19 structures exhibit a large $|\lambda_2 - 1|$ (>0.051). They are mainly found in the Ni–Ti–X alloys with less energetic stability of the martensitic-phase structures than the phase-separation states (Fig. 7), such as $Ni_{37.5}Ti_{50}X_{12.5}$ alloys with X of alkali and alkaline earth metal elements, and

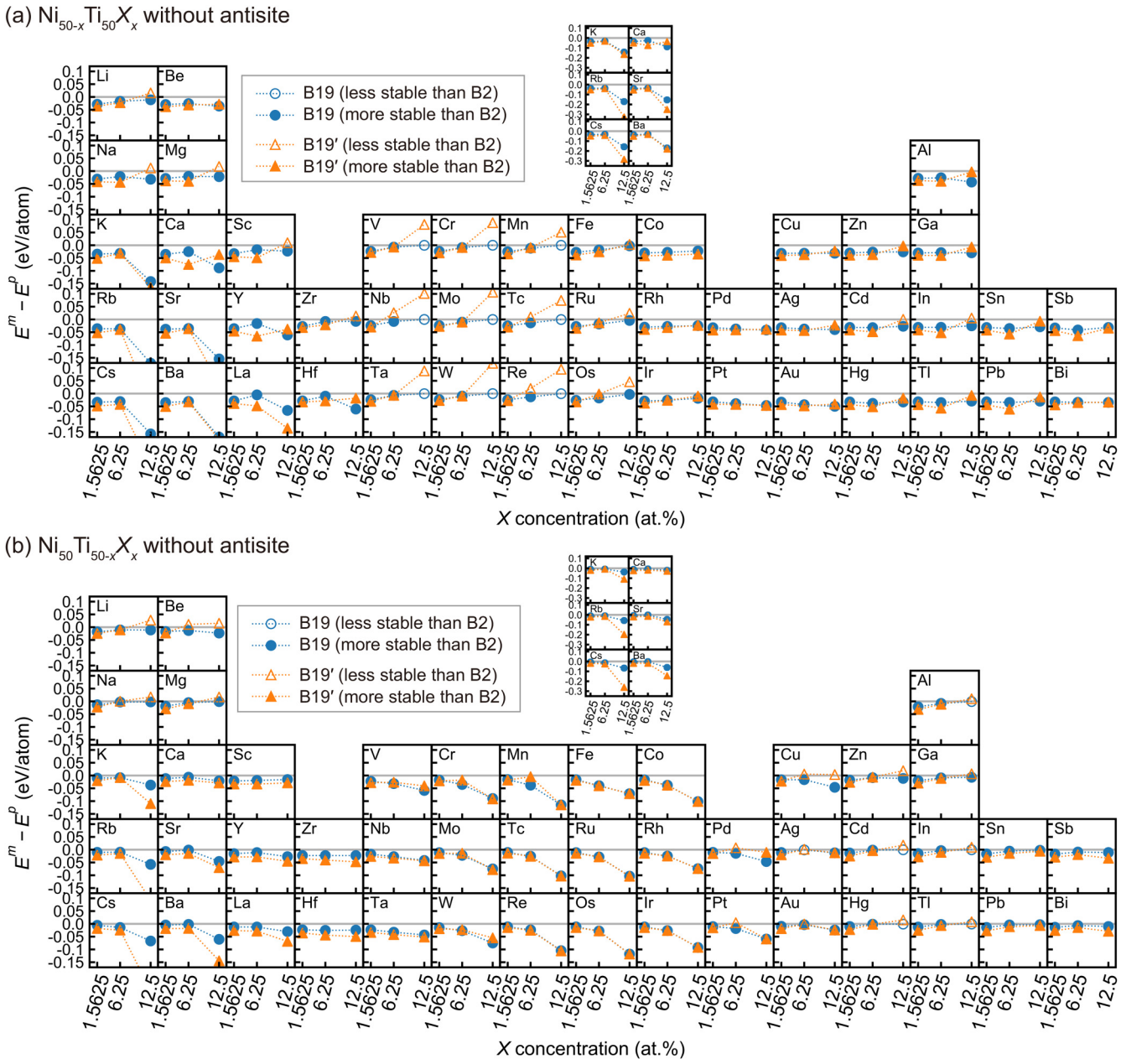

FIG. 5. Energy differences between the martensitic-phase and B2 parent-phase structures in the ternary Ni–Ti–*X* alloys under the (a) Ni-deficient and (b) Ti-deficient conditions when *X* occupies the deficient-element site. Blue circles and orange triangles indicate the B19 and B19′ structures, respectively, and dotted lines connecting the symbols are guides for the eyes. Filled symbols indicate that the martensitic-phase structure is energetically more stable than the B2 structure. Note that for 15 alloys, both the B19 and B19′ structures are energetically less stable than the B2 parent-phase structure, which indicates that the shape memory effects may be lost. The figures are drawn again with a larger range of *y*-axes at the upper center space for *X* in groups 1–2 and periods 4–6.

therefore are probably not found in experiments. The B19 structure of $Ni_{37.5}Ti_{50}Hf_{12.5}$ also has much larger $|\lambda_2 - 1|$ than the B19′ structure. It is found that the B19 structure of $Ni_{37.5}Ti_{50}Hf_{12.5}$, which should be orthorhombic, actually converged into a tetragonal structure after the structural optimization.

Figure 9 shows the computed $\det(\mathbf{U}) - 1$ of the 276 Ni–Ti–X alloys. As with $|\lambda_2 - 1|$, for many (209 out of 276) of

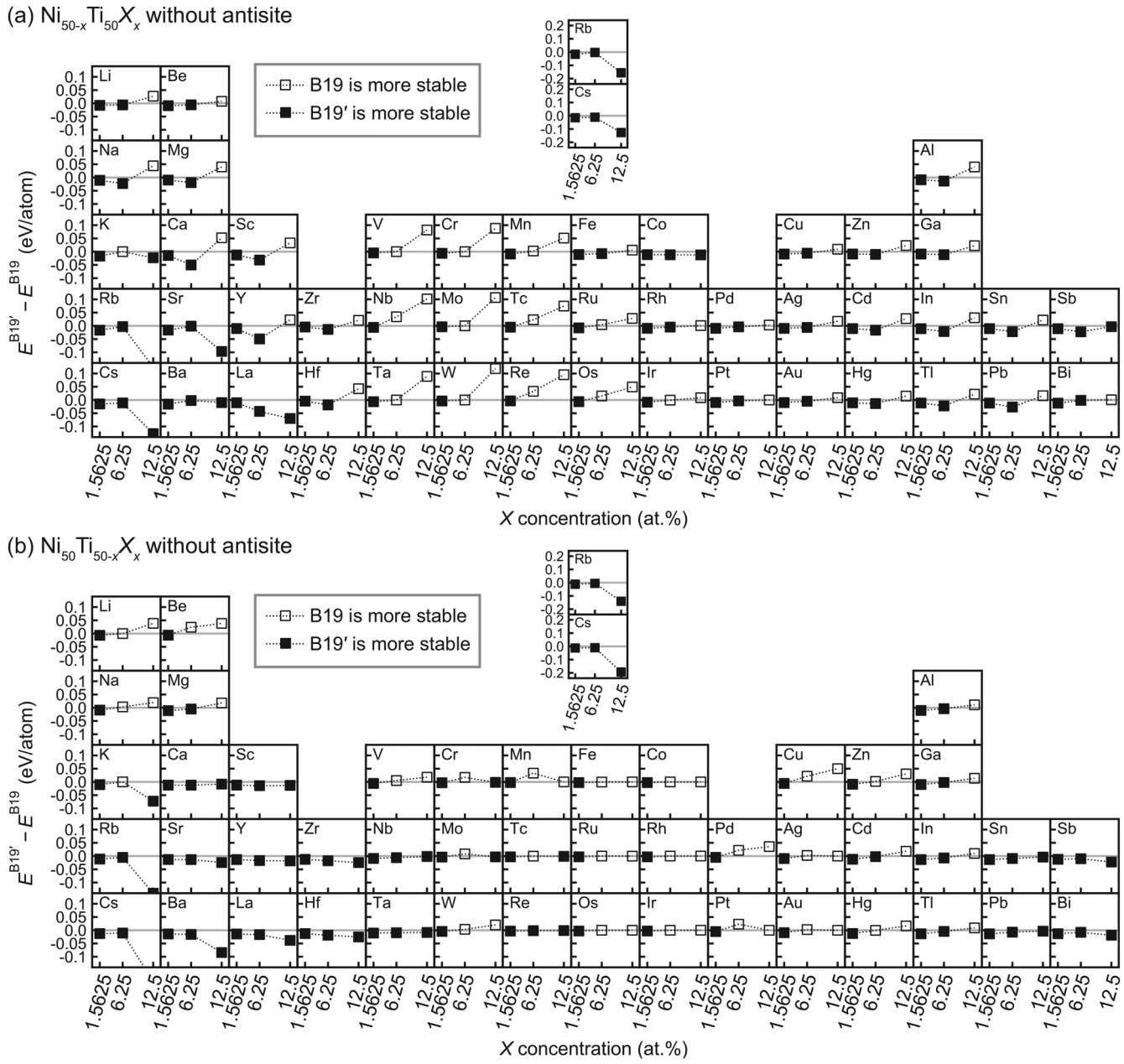

FIG. 6. Energy differences between the martensitic-phase structures in the ternary Ni–Ti–*X* alloys under the (a) Ni-deficient and (b) Ti-deficient conditions when *X* occupies the deficient-element site. Filled and open symbols indicate that the B19′ and B19 structures are energetically more stable than the other, respectively. Dotted lines connecting the symbols are guides for the eyes. The figures are drawn again with a wider range of *y*-axes at the upper center space for *X* of Rb and Cs.

the Ni–Ti–X alloys, the $|\det(\mathbf{U})-1|$ values of the B19 structures are also smaller than those of the B19′ structures. If $|\det(\mathbf{U})-1|$ is large, huge stress may occur during the transformation.[40] In the present calculations, the $Ni_{37.5}Ti_{50}X_{12.5}$ and $Ni_{50}Ti_{37.5}X_{12.5}$ alloys with X = K, Rb, Cs, Ca, Sr, or Ba have $|\det(\mathbf{U})-1|$ over 0.05, which is much larger than those of the other Ni–Ti–X alloys. Therefore, it is expected that these alloys have poor functional stability as SMAs even if they have λ_2 close to one and therefore show good structural compatibility.

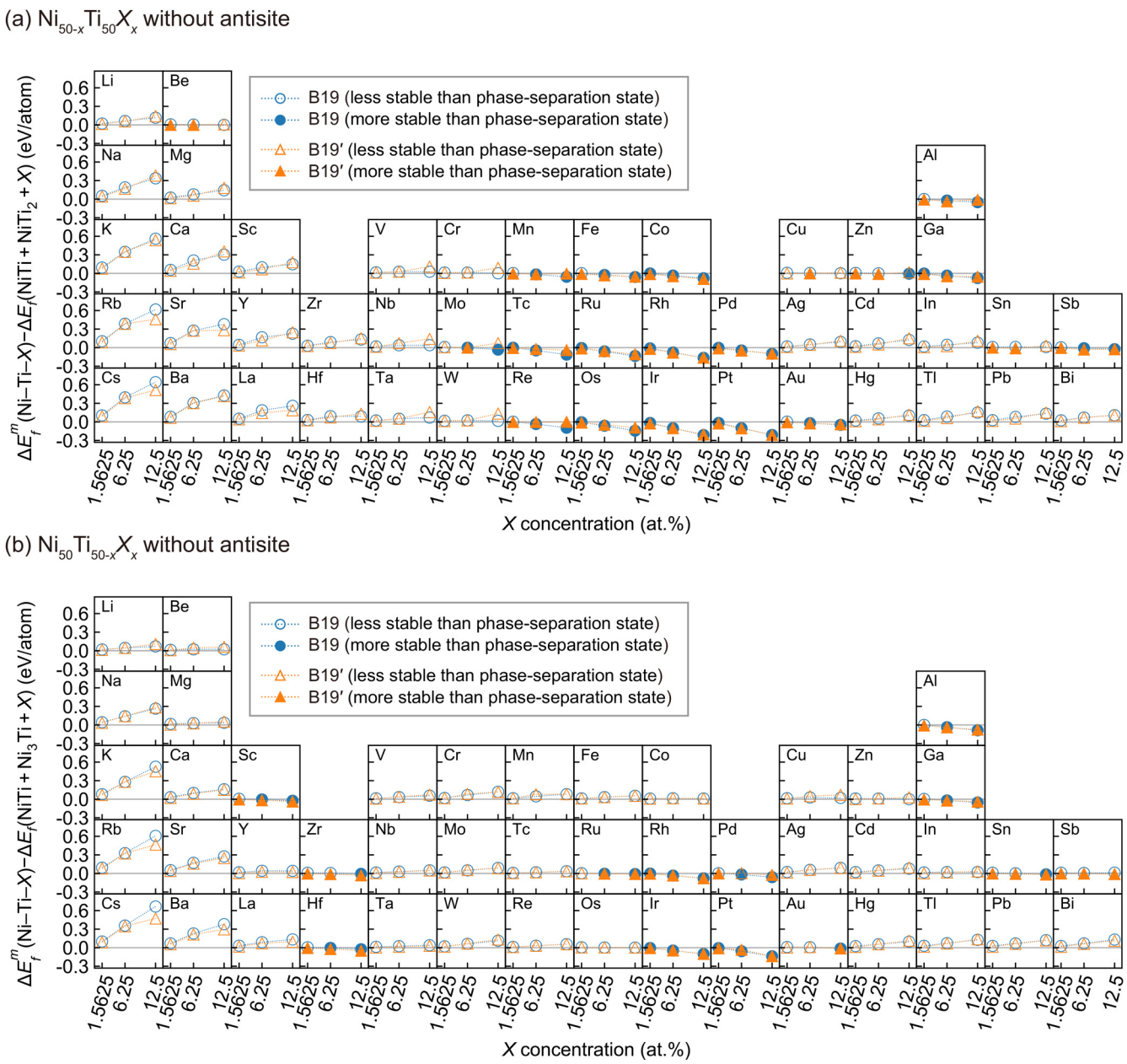

FIG. 7. Energies of the martensitic-phase structures of the ternary Ni–Ti–*X* alloys (a) under the Ni-deficient condition, where the energies are compared with those of NiTi + $NiTi_2$ + *X*, and (b) under the Ti-deficient condition, where the energies are compared with those of NiTi + Ni_3Ti + *X*. The deficient-element site is occupied by *X*. Filled symbols indicate that the martensitic-phase structure is energetically more stable than the phase-separation state. Dotted lines are guides for the eyes.

The comparisons of $\lambda_2 - 1$ and $\det(\mathbf{U}) - 1$ between the two martensitic-phase structures reveal that the B19 structure tends to be preferred to the B19′ structure from the viewpoint of the structural compatibility with the parent-phase structure for most of the investigated alloys. Unlike the B19–B2 transformation, the B19′–B2 transformation needs an additional nonbasal lattice shear,[10,41] which is directly related to γ larger than 90°. Figure 10 shows the relationship between the $\gamma - 90°$ and $\lambda_2 - 1$ of the B19′ structures of the investigated Ni–Ti–X alloys. Here, we analyze the 177 B19′ structures that are energetically more stable than the B2 and the B19 structures and retain the monoclinic symmetry.

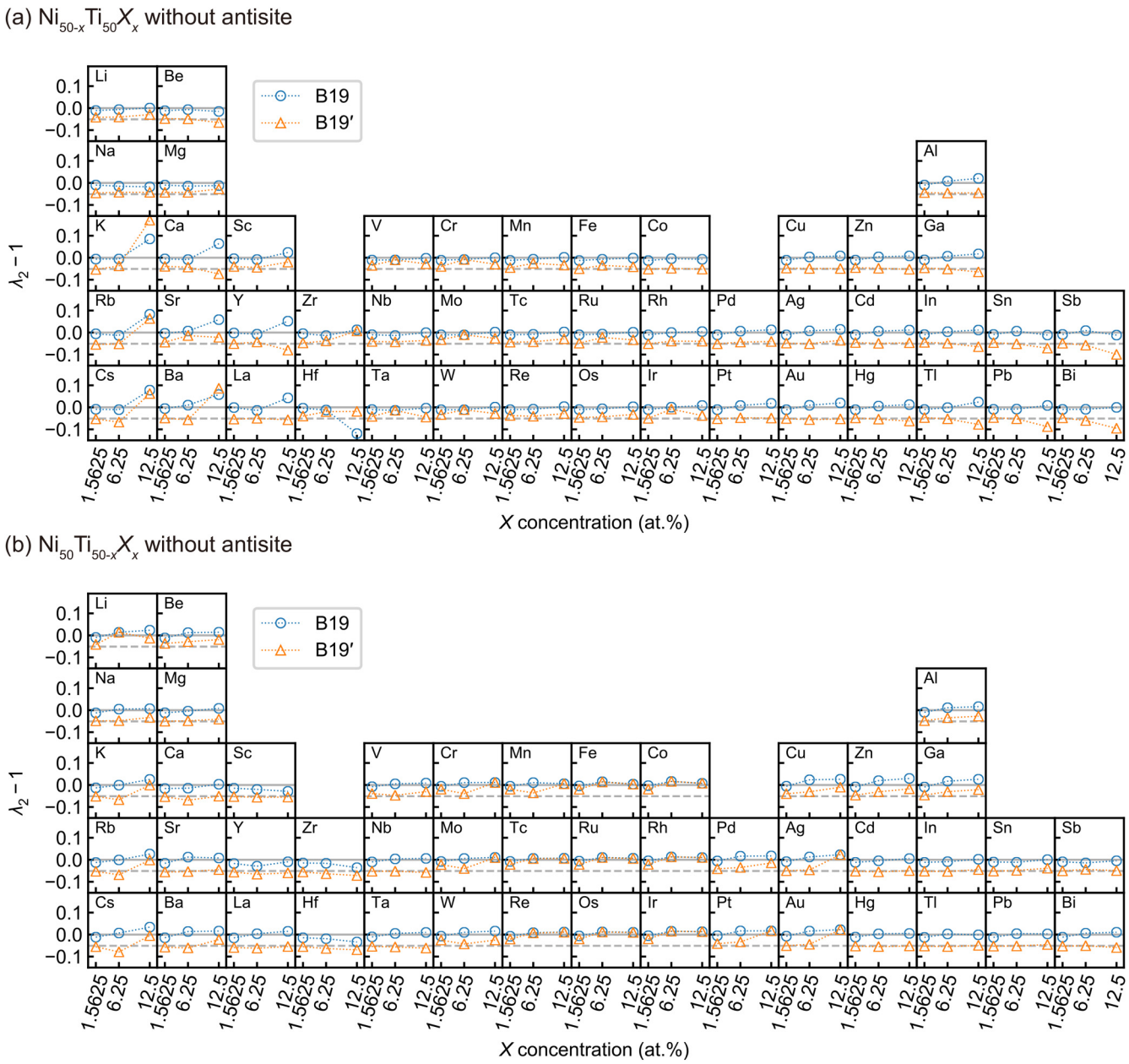

FIG. 8. $\lambda_2 - 1$ of the ternary Ni–Ti–*X* alloys under the (a) Ni-deficient and (b) Ti-deficient conditions when *X* occupies the deficient-element site. Blue circles and orange triangles indicate the B19 and B19′ structures, respectively. Dashed horizontal lines indicate $\lambda_2 - 1$ of the binary equiatomic NiTi between the B2 and B19′ structures (−0.051). Dotted lines connecting the symbols are guides for the eyes.

We confirm that Pearson's and Spearman's rank correlation coefficients[42] of γ and $|\lambda_2 - 1|$ in Fig. 10 are 0.56 and 0.71, respectively. This indicates that the monoclinic angle γ and $|\lambda_2 - 1|$ have a correlation for the B19′ structure of Ni–Ti–X alloys. Indeed, only 6 out of the 177 B19′ structures have γ smaller than 95° and $|\lambda_2 - 1|$ smaller than 0.014, whereas the other B19′ structures have larger γ as well as larger $|\lambda_2 - 1|$. Note that the three $Ni_{50}Ti_{37.5}X_{12.5}$ alloys with K, Rb, and Cs as X have the B19′ structures with both γ larger than 100° and $|\lambda_2 - 1|$ less than 0.02. These alloys are energetically less stable than the phase-separation states (see Fig. 7) and may cause a phase transition or a phase separation.

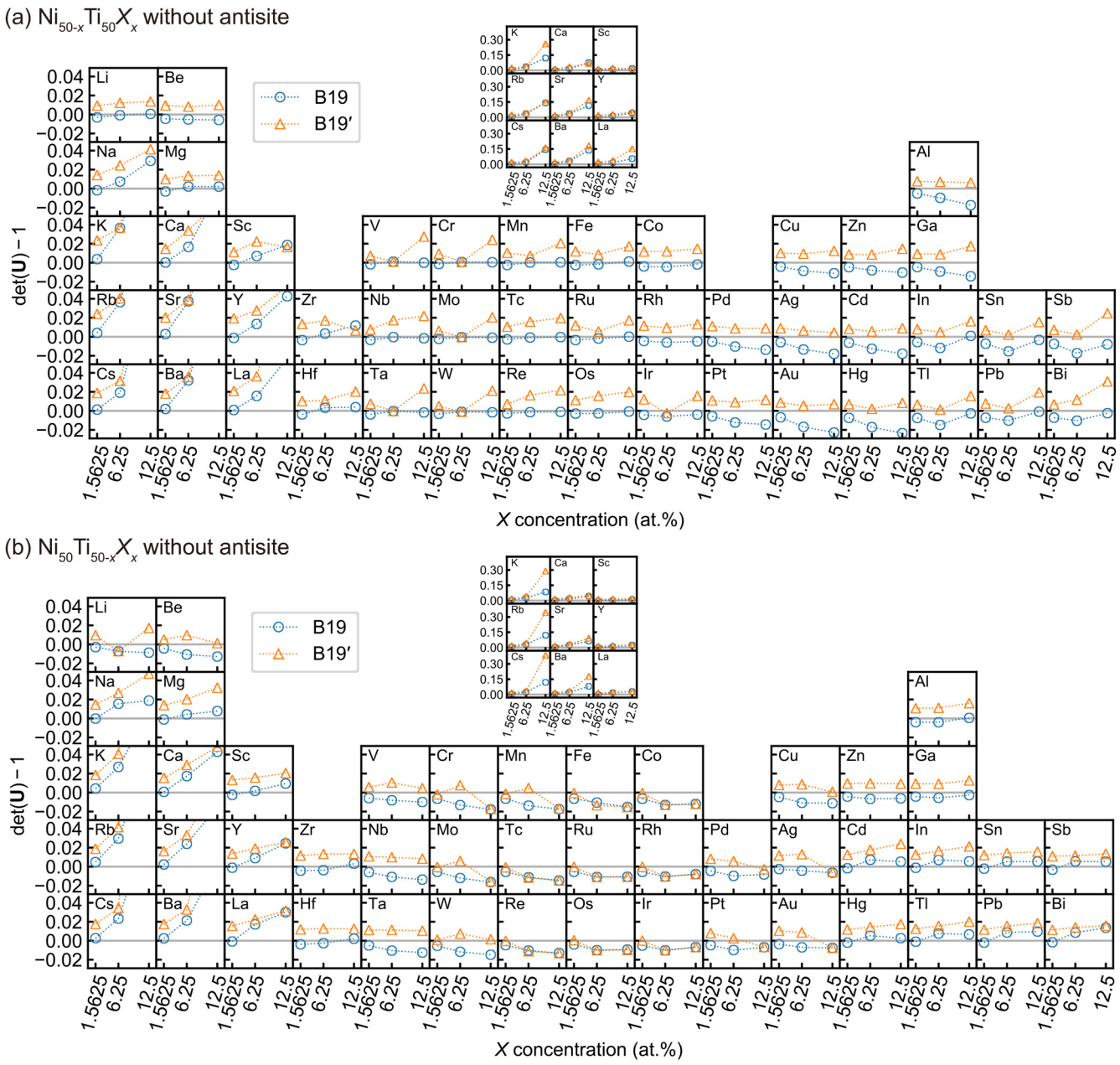

FIG. 9. det(**U**) − 1 of the ternary Ni–Ti–*X* alloys under the (a) Ni-deficient and (b) Ti-deficient conditions when *X* occupies the deficient-element site. Blue circles and orange triangles indicate the B19 and B19′ structures, respectively. Dotted lines connecting the symbols are guides for the eyes. The figures are drawn again with a wider range of *y*-axes at the upper center space for *X* in groups 1–3 and periods 4–6.

As described in Sec. III D, some X can energetically stabilize the B19 structure more than the B19′ structure, and such alloys can also be energetically more stable than the considered phase-separation states. The combination of the results indicates that the structural compatibility of NiTi-based alloys, and therefore their functional stability, can be improved by energetically stabilizing the B19 martensitic-phase structure by alloying. Actually, in experiments, $Ti_{50.2}Ni_{34.4}Cu_{12.3}Pd_{3.1}$ (Ref. 5) and $Ti_{54}Ni_{34}Cu_{12}$ (Ref. 43) show the B19–B2 transformation and low functional fatigue.

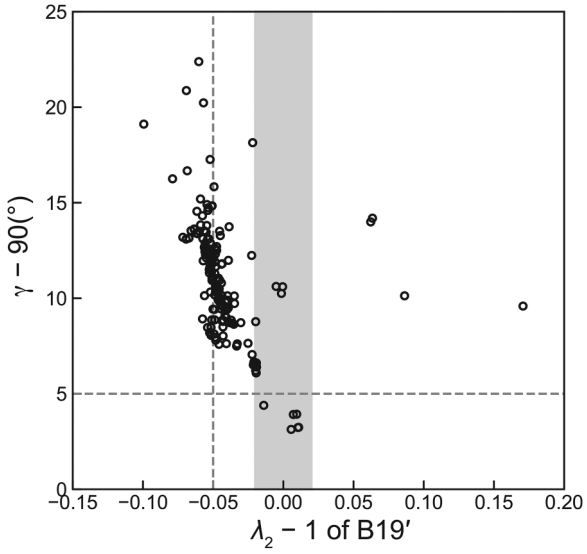

FIG. 10. Relationship between the monoclinic angle γ of the B19′ structure and $\lambda_2 - 1$ of the B19′–B2 transformation for the 177 Ni–Ti–*X* alloys where the B19′ structure is energetically the most stable among the investigated crystal structures. The gray vertical band denotes $|\lambda_2 - 1| \leq 0.02$, and the dashed gray vertical line denotes $\lambda_2 - 1$ of the binary equiatomic NiTi (−0.051). The gray horizontal dashed line denotes γ of 95°. Among the 177 B19′ structures, only six have γ smaller than 95° with $|\lambda_2 - 1|$ less than 0.014.

Our computational results are also consistent with experimental findings previously reported. In experiments, $Ni_{50-x}Ti_{50}Cu_x$ shows the B19′–B2 and B19–B2 transformations for $x < 7.7$ and $x \geq 7.7$, respectively.[44] Moreover, the $|\lambda_2 - 1|$ values of $Ni_{50-x}Ti_{50}Cu_x$ and $Ni_{50-x}Ti_{50}Pd_x$ alloys are less than ~0.01 when x is around 7–20 and 7–25 at. %, respectively.[3] Our calculations reveal that in $Ni_{50-x}Ti_{50}Cu_x$ and $Ni_{50-x}Ti_{50}Pd_x$ with $x = 1.5625$ or 6.25, the B19′ structures are energetically more stable than the B19 structures and have large $|\lambda_2 - 1|$ of more than ~0.05 for the B19′–B2 transformation, but in the alloys with $x = 12.5$, the B19 structures are energetically more stable than the B19′ structures and have much smaller $|\lambda_2 - 1|$ of less than ~0.02 for the B19–B2 transformation. It is also reported in experiments that $Ni_{50}Ti_{50-x}Hf_x$ with $8 < x < 20$ has the B19′ martensitic-phase structure,[45] and larger thermal hysteresis (>60 °C) and $|\lambda_2 - 1|$ (>~0.03 in experimental value) than those of the binary equiatomic NiTi.[3] This is consistent with our computational result that for the $Ni_{50}Ti_{50-x}Hf_x$ alloys, the B19′ structure is energetically more stable than the B19 structure, and $|\lambda_2 - 1|$ of the B19′–B2 transformation is larger than that of the binary equiatomic NiTi at all the investigated concentrations of Hf.

F. Chemical elements with better energetic and structural properties as Ni–Ti–*X* SMAs

In Figs. 5–9 in Secs. III D and III E, we detailed the energetic and structural properties of the 276 ternary Ni–Ti–X alloys using the $\min\{E^{B19}(\text{Ni–Ti–X}), E^{B19'}(\text{Ni–Ti–X})\} - E^{B2}(\text{Ni–Ti–X})$, $\Delta E_f^m(\text{Ni–Ti–X}) - \Delta E_f(\text{phase-separation state})$, $|\lambda_2 - 1|$, and $|\det(\mathbf{U}) - 1|$. We summarize these properties as the screening conditions for the $Ni_{50-x}Ti_{50}X_x$ alloys in Fig. 11 and for the $Ni_{50}Ti_{50-x}X_x$ alloys in Fig. 12. We employed the following two criteria for $|\lambda_2 - 1|$. The first criterion is whether $|\lambda_2 - 1|$ of the Ni–Ti–X alloys is smaller than that of the binary equiatomic NiTi (0.051), which is for finding the Ni–Ti–X alloys with better structural compatibility than the binary equiatomic NiTi. The second criterion is whether $|\lambda_2 - 1|$ of the Ni–Ti–X alloys is smaller than 0.02, which is much smaller than that of the binary equiatomic NiTi. This is for finding the Ni–Ti–X alloys with thermal hysteresis much smaller than that of the binary equiatomic NiTi as 50–60 K.[3,4] We also employed another criterion for the structural property, whether $|\det(\mathbf{U}) - 1|$ is smaller than 0.02, to avoid the alloys with a large volume change caused by the martensitic transformation.

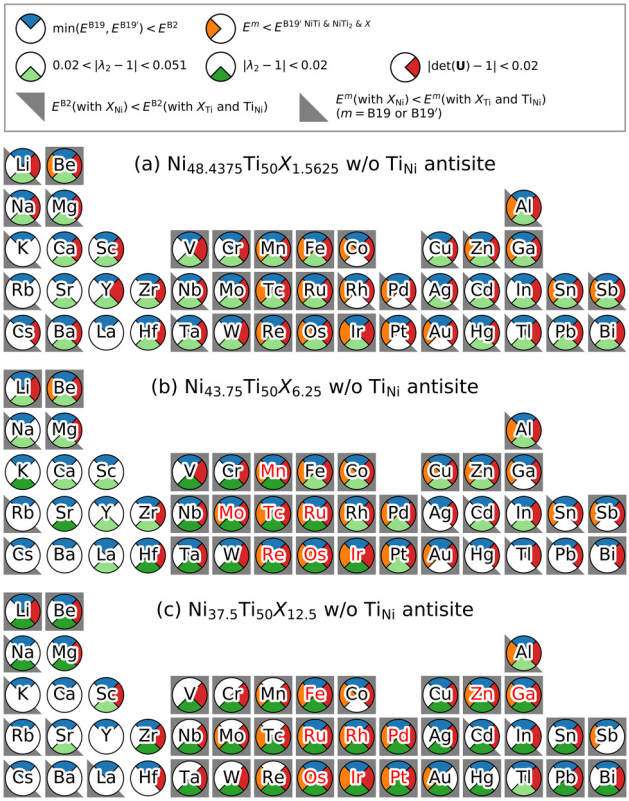

FIG. 11. Screening of $Ni_{50-x}Ti_{50}X_x$ alloys when *X* of (a) 1.5625 at. %, (b) 6.25 at. %, or (c) 12.5 at. % occupies the deficient-element site under the conditions of structural compatibility between parent-phase (B2) and martensitic-phase (B19 and B19′) structures, and energetic stability employed in Figs. 5–9. The screening conditions summarized in the legend are displayed as different sectors in the circles. The *X* satisfying all of the screening conditions in the $Ni_{50-x}Ti_{50}X_x$ alloys are shown as red text. The site preferences in energy (shown in Figs. 3 and 4) are separately displayed as gray triangles on the background.

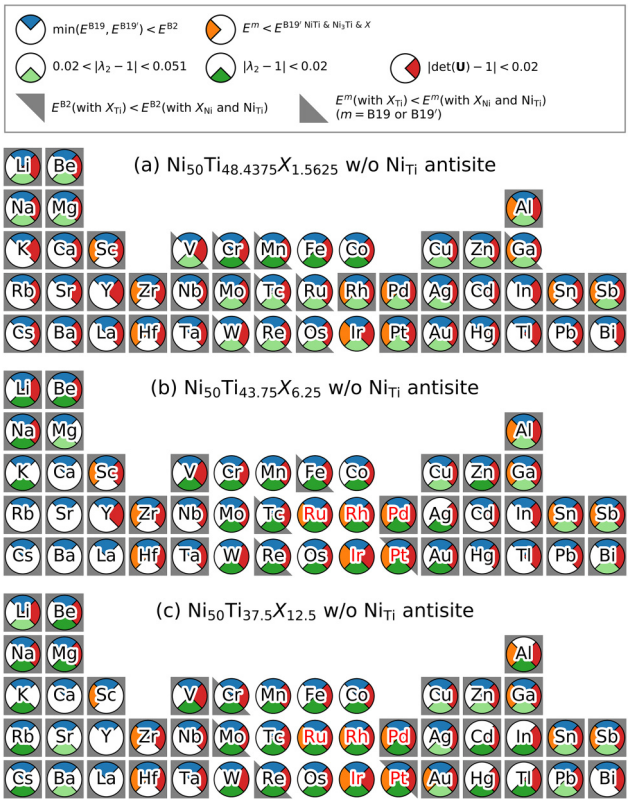

FIG. 12. Screening of $Ni_{50}Ti_{50-x}X_x$ alloys when X of (a) 1.5625 at. %, (b) 6.25 at. %, or (c) 12.5 at. % occupies the deficient-element site. The other details are the same as in Fig. 11.

From the 276 Ni–Ti–X alloys, 199 (a large proportion of) alloys show smaller $|\lambda_2 - 1|$ than the binary equiatomic NiTi. It is found that 180 out of the 199 alloys also satisfy $|\det(\mathbf{U}) - 1| < 0.02$. However, when the energetic screening conditions of $\min\{E^{B19}(\text{Ni–Ti–X}), E^{B19'}(\text{Ni–Ti–X})\} < E^{B2}(\text{Ni–Ti–X})$ and $\Delta E_f^m(\text{Ni–Ti–X}) < \Delta E_f(\text{phase-separation state})$ are added, the number of alloys simultaneously satisfying the above conditions significantly decrease to 64. This implies that the energetic-stability conditions largely limit the suitability of alloys as SMAs.

It is found that 26 Ni–Ti–X alloys satisfy $|\lambda_2 - 1| < 0.02$, $|\det(\mathbf{U}) - 1| < 0.02$, $\min\{E^{B19}(\text{Ni–Ti–X}), E^{B19'}(\text{Ni–Ti–X})\} < E^{B2}(\text{Ni–Ti–X})$, and $\Delta E_f^m(\text{Ni–Ti–X}) < \Delta E_f(\text{phase-separation state})$ simultaneously. These surviving alloys consist of 16 Ni-deficient alloys and 10 Ti-deficient alloys. All of the 16 Ni-deficient alloys also satisfy $E(\text{with } X_{Ni}) < E(\text{with } X_{Ti} \text{ and } Ti_{Ni})$. However, among the 10 Ti-deficient alloys, only the $Ni_{50}Ti_{43.75}Pd_{6.25}$ and $Ni_{50}Ti_{37.5}Pd_{12.5}$ alloys also satisfy $E(\text{with } X_{Ti}) < E(\text{with } X_{Ni} \text{ and } Ni_{Ti})$ for both the B2 parent-phase and martensitic-phase structures. In the other 8 Ti-deficient alloys, namely, $Ni_{50}Ti_{43.75}X_{6.25}$ and $Ni_{50}Ti_{37.5}X_{12.5}$ with X = Ru, Rh, Ir, or Pt, the alloyed element X energetically prefers to occupy the rich-element site, creating the rich-element antisite rather than occupy the deficient-element site in either or both the B2 parent-phase and martensitic-phase structures. For these alloys, further investigation on the structural compatibility between the parent-phase and martensitic-phase structures may be needed using, for example, the models including the antisite. Furthermore, for the $Ni_{50}Ti_{43.75}Pt_{6.25}$ and $Ni_{50}Ti_{37.5}Pt_{12.5}$ alloys, where the site preference of Pt is different between those in the B2 parent-phase and martensitic-phase structures, we also need to be careful with the occupied site of Pt during the martensitic transformation, probably by also considering the atomic diffusion. These cases are beyond the scope of this study, which is mainly aimed at the structural compatibility of NiTi-based alloys, and are not discussed hereafter.

We find that the $Ni_{37.5}Ti_{50}Pd_{12.5}$ and $Ni_{37.5}Ti_{50}Pt_{12.5}$ alloys survive in the above screening among the $Ni_{50-x}Ti_{50}X_x$ (X = Cu, Pd, Pt, or Au) alloys, which are known to show a smaller thermal hysteresis in experiments.[3] On the other hand, the $Ni_{37.5}Ti_{50}Cu_{12.5}$ and $Ni_{37.5}Ti_{50}Au_{12.5}$ alloys are not included in the 26 surviving alloys. For the $Ni_{37.5}Ti_{50}Cu_{12.5}$ alloy, the martensitic-phase structure is energetically less stable than the phase-separation state, which implies that this alloy may exist as a metastable phase in experiments. The $Ni_{37.5}Ti_{50}Au_{12.5}$ alloy does not satisfy the condition $|\det(\mathbf{U}) - 1| < 0.02$, which means that the volume change can be large during the martensitic transformation.

The $Ni_{37.5}Ti_{50}Fe_{12.5}$ alloy also survives from our screening, although, to the best of our knowledge, this alloy has not been reported as a SMA with better functional stability than the binary equiatomic NiTi. This is probably because other phases that were not investigated in this study are energetically more stable than the B19 structure. In experiments, $Ni_{50-x}Ti_{50}Fe_x$ alloys with $2 < x < 3$ have actually been shown to undergo the two-stage martensitic transformation between the B2 and trigonal R phases and between the R and B19′ phases,[46–48] whereas in the alloys with $x > 6$, these transformations disappear, and instead, other phases, called the commensurate and incommensurate phases, appear at low temperature.[49–51] In principle, such phases can also be considered in the screening, but this is beyond the scope of this study that is aimed at the systematic investigation of the impact of the different alloying elements.

Before concluding, we should point out that detailed energy balances and structural parameters may be more or less modified due to the temperature effect. Actually, the monoclinic angle γ in the B19′ structure of binary equiatomic NiTi was shown to decrease when increasing temperature using classical MD simulations with first-principles-derived interatomic potentials[26] and using first-principles MD simulations.[14] Nevertheless, we expect the chemical and the compositional trends are not largely varied from the current results for 0 K, as found from the above-mentioned consistency with the experimental findings. It is also worth noting that the martensitic-transformation properties of binary equiatomic NiTi such as the transformation temperature and the reversibility also depend on its nanostructures. Classical MD simulations using first-principles-derived interatomic potentials

revealed that the martensitic transformation temperatures of nanocrystalline, nanoprecipitate, and freestanding nanoparticle binary equiatomic NiTi are affected by its grain size,[52] its matrix composition ratio,[53] and its particle size,[54] respectively. The current screening results are expected to be also helpful when extending such nanostructure analyses to the Ni–Ti alloys with the addition of other elements.

IV. CONCLUSION

We performed systematic first-principles calculations to investigate the dependences of the energetics and structural properties of Ni–Ti–X alloys on the substituted chemical element X, the X concentration, and the replaced chemical element (Ni or Ti). In particular, we focused on the energetic stability of the more stable martensitic-phase structure against possible phase-separation states, the phase stabilities of the B19 and B19′ martensitic-phase structures against the B2 parent-phase structure, and the structural compatibility between the parent-phase and the martensitic-phase structures.

For binary nonstoichiometric Ni–Ti alloys, we find that the B19 structure can be energetically more stable than the B19′ structure, and their $|\lambda_2 - 1|$ can be smaller than that of the binary equiatomic NiTi. However, these nonstoichiometric alloys are also found to be energetically less stable than possible phase-separation states. This indicates that it may be difficult to improve the functional stability, which is ascribed to the structural compatibility of NiTi, by merely modifying their composition ratios, and therefore, alloying with additional elements may be essential.

For the ternary Ni–Ti–X alloys, we first analyzed the site preference of X under both the Ni-deficient and Ti-deficient conditions. Our results are mostly consistent with experimental observations and previous computational findings for the B2 parent-phase structure. Furthermore, we find that for some X, the site preference is different between the B2 and martensitic-phase structures.

From the comparative analysis between the parent and martensitic phases, it is found that some types of X energetically stabilize the B19 structure more than the B19′ structure when X is included at 6.25 at. % or more. It is also found that for most of the Ni–Ti–X alloys, the B19–B2 transformation show smaller $|\lambda_2 - 1|$ than the B19′–B2 transformation. Most such alloys show smaller $|\lambda_2 - 1|$ than that of the binary equiatomic NiTi, which verifies the strong potential to improve the functional stability of Ni–Ti SMAs by alloying. Our computational results are consistent with the experimental finding that some ternary alloys with good functional stability, such as $Ni_{43}Ti_{50}Pd_x$ ($x > 7$),[3] have the B19 martensitic-phase structure and have good structural compatibility.

We finally screen the investigated ternary Ni–Ti–X alloys on the basis of their energetic stability and structural compatibility between the parent and martensitic phases, and we identify 26 Ni–Ti–X alloys that have better energetic stability than these phase-separation states and small $|\lambda_2 - 1|$ (less than 0.02) simultaneously. Some of the 26 alloys are actually known to show shape memory effects with better functional stability than the binary equiatomic NiTi. The present work demonstrates a method of the computational design of SMAs with good functional stability by alloying additional elements.

SUPPLEMENTARY MATERIAL

The information of comparison of the B19′ and the B33 structures for computed Ni–Ti(–X) alloys can be found in the supplementary material.

ACKNOWLEDGMENTS

This work was supported by Grant-in-Aid for Scientific Research (A) and Grant-in-Aid for Scientific Research on Innovative Areas "Nano Informatics" (Grant No. 25106005) from the Japan Society for the Promotion of Science (JSPS), and Support program for starting up innovation hub on "Materials Research by Information Integration" Initiative from Japan Science and Technology Agency. J.L. acknowledges Grant-in-Aid for International Research Fellow of JSPS (Grant No. 2604376) and JSPS fellowships. Y.I. acknowledges Grant-in-Aid for Young Scientist (B) of JSPS (Grant No. 16K18228). Funding by the Ministry of Education, Culture, Sports, Science and Technology (MEXT), Japan, through Elements Strategy Initiative for Structural Materials (ESISM) of Kyoto University, is also gratefully acknowledged.

REFERENCES

[1]J. M. Jani, M. Leary, A. Subic, and M. A. Gibson, Mater. Design **56**, 1078 (2014).
[2]K. Otsuka and X. Ren, Prog. Mater. Sci. **50**, 511 (2005).
[3]Z. Zhang, R. D. James, and S. Müller, Acta Mater. **57**, 4332 (2009).
[4]J. Cui, Y. S. Chu, O. O. Famodu, Y. Furuya, J. Hattrick-Simpers, R. D. James, A. Ludwig, S. Thienhaus, M. Wuttig, Z. Zhang, and I. Takeuchi, Nat. Mater. **5**, 286 (2006).
[5]R. Zarnetta, R. Takahashi, M. L. Young, A. Savan, Y. Furuya, S. Thienhaus, B. Maaß, M. Rahim, J. Frenzel, H. Brunken, Y. S. Chu, V. Srivastava, R. D. James, I. Takeuchi, G. Eggeler, and A. Ludwig, Adv. Func. Mater. **20**, 1917 (2010).
[6]R. D. James and K. F. Hane, Acta Mater. **48**, 197 (2000).
[7]K. Otsuka, T. Sawamura, and K. Shimizu, Phys. Status Solidi A **5**, 457 (1971).
[8]Y. Kudoh, M. Tokonami, S. Miyazaki, and K. Otsuka, Acta Metall. **33**, 2049 (1985).
[9]X. Huang, G. J. Ackland, and K. M. Rabe, Nat. Mater. **2**, 307 (2003).
[10]S. Kibey, H. Sehitoglu, and D. D. Johnson, Acta Mater. **57**, 1624 (2009).
[11]K. G. Vishnu and A. Strachan, Acta Mater. **58**, 745 (2010).
[12]D. Holec, M. Friák, A. Dlouhý, and J. Neugebauer, Phys. Rev. B **84**, 224119 (2011).
[13]M. Mizuno, H. Araki, and Y. Shirai, Acta Mater. **95**, 184 (2015).
[14]J. B. Haskins, A. E. Thompson, and J. W. Lawson, Phys. Rev. B **94**, 214110 (2016).
[15]J. B. Haskins and J. W. Lawson, J. Appl. Phys. **121**, 205103 (2017).
[16]N. A. Zarkevich and D. D. Johnson, Phys. Rev. Lett. **113**, 265701 (2014).
[17]N. Hatcher, O. Y. Kontsevoi, and A. J. Freeman, Phys. Rev. B **80**, 144203 (2009).
[18]M. F. X. Wagner and W. Windl, Acta Mater. **56**, 6232 (2008).
[19]J. M. Lu, Q. M. Hu, L. Wang, Y. J. Li, D. S. Xu, and R. Yang, Phys. Rev. B **75**, 094108 (2007).
[20]M. E. Manley, M. Asta, J. C. Lashley, C. M. Retford, W. L. Hults, R. D. Taylor, D. J. Thoma, J. L. Smith, R. E. Hackenberg, and K. Littrell, Phys. Rev. B **77**, 024201 (2008).

[21]D. Holec, M. Friák, A. Dlouhý, and J. Neugebauer, Phys. Rev. B **89**, 014110 (2014).
[22]J. Frenzel, A. Wieczorek, I. Opahle, B. Maaß, R. Drautz, and G. Eggeler, Acta Mater. **90**, 213 (2015).
[23]N. Singh, A. Talapatra, A. Junkaew, T. Duong, S. Gibbons, S. Li, H. Thawabi, E. Olivos, and R. Arróyave, Comput. Mater. Sci. **112**, 347 (2016).
[24]Z. Nishiyama, *Martensitic Transformation*, 1st ed. (Academic Press, 1978).
[25]J. Lee, Y. Ikeda, and I. Tanaka, NPJ Comput. Mater. **3**, 52 (2017).
[26]W.-S. Ko, B. Grabowski, and J. Neugebauer, Phys. Rev. B **92**, 134107 (2015).
[27]X. Huang, C. Bungaro, V. Godlevsky, and K. M. Rabe, Phys. Rev. B **65**, 014108 (2001).
[28]K. Parlinski and M. Parlinska-Wojtan, Phys. Rev. B **66**, 064307 (2002).
[29]P. Souvatzis, D. Legut, O. Eriksson, and M. I. Katsnelson, Phys. Rev. B **81**, 092201 (2010).
[30]N. A. Zarkevich and D. D. Johnson, Phys. Rev. B **90**, 060102 (2014).
[31]P. E. Blöchl, Phys. Rev. B **50**, 17953 (1994).
[32]G. Kresse and D. Joubert, Phys. Rev. B **59**, 1758 (1999).
[33]G. Kresse and J. Furthmüller, Comput. Mater. Sci. **6**, 15 (1996).
[34]G. Kresse and J. Furthmüller, Phys. Rev. B **54**, 11169 (1996).
[35]J. P. Perdew, K. Burke, and M. Ernzerhof, Phys. Rev. Lett. **77**, 3865 (1996).
[36]M. Methfessel and A. T. Paxton, Phys. Rev. B **40**, 3616 (1989).
[37]J. M. G. Fuentes, P. Gümpel, and J. Strittmatter, Adv. Eng. Mater. **4**, 437 (2002).
[38]G. Bozzolo, R. D. Noebe, and H. O. Mosca, J. Alloys Compd. **386**, 125 (2005).
[39]G. Bozzolo, R. D. Noebe, and H. O. Mosca, J. Alloys Compd. **389**, 80 (2005).
[40]R. D. James and Z. Zhang, in *Magnetism and Structure in Functional Materials*, edited by A. Planes, L. Mañosa, and A. Saxena (Springer, Heidelberg, 2005), p. 159.
[41]K. Otsuka and X. Ren, Mater. Sci. Eng. A **273**, 89 (1999).
[42]J. D. Evans, *Straightforward Statistics for the Behavioral Sciences* (Brooks/Cole, 1996).
[43]C. Chluba, W. Ge, R. L. de Miranda, J. Strobel, L. Kienle, E. Quandt, and M. Wuttig, Science **348**, 1004 (2015).
[44]W. Tang, R. Sandstrom, Z. G. Wei, and S. Miyazaki, Metall. Mater. Trans. A **31**, 2423 (2000).
[45]P. L. Potapov, A. V. Shelyakov, A. A. Gulyaev, E. L. Svistunov, N. M. Matveeva, and D. Hodgson, Mater. Lett. **32**, 247 (1997).
[46]J. J. Wang, T. Omori, Y. Sutou, R. Kainuma, and K. Ishida, Scr. Mater. **52**, 311 (2005).
[47]J. Frenzel, J. Pfetzing, K. Neuking, and G. Eggeler, Mater. Sci. Eng. A **481–482**, 635 (2008).
[48]I. Yoshida, D. Monma, and T. Ono, J. Alloys Compd. **448**, 349 (2008).
[49]M. S. Choi, T. Fukuda, T. Kakeshita, and H. Mori, Philos. Mag. **86**, 67 (2006).
[50]M.-S. Choi, T. Fukuda, and T. Kakeshita, Scr. Mater. **53**, 869 (2005).
[51]M.-S. Choi, T. Yamamoto, T. Fukuda, T. Kakeshita, E. Taguchi, and H. Mori, Philos. Mag. **88**, 2449 (2008).
[52]W.-S. Ko, S. B. Maisel, B. Grabowski, J. B. Jeon, and J. Neugebauer, Acta Mater. **123**, 90 (2017).
[53]S. B. Maisel, W. S. Ko, J. L. Zhang, B. Grabowski, and J. Neugebauer, Phys. Rev. Mater. **1**, 033610 (2017).
[54]W.-S. Ko, B. Grabowski, and J. Neugebauer, Phys. Rev. Mater. **2**, 030601 (2018).
[55]S. D. Prokoshkin, A. V. Korotitskiy, V. Brailovski, S. Turenne, I. Y. Khmelevskaya, and I. B. Trubitsyna, Acta Mater. **52**, 4479 (2004).
[56]D. Vanderbilt, Phys. Rev. B **41**, 7892 (1990).
[57]E. Wimmer, H. Krakauer, M. Weinert, and A. J. Freeman, Phys. Rev. B **24**, 864 (1981).
[58]J. P. Perdew, J. A. Chevary, S. H. Vosko, K. A. Jackson, M. R. Pederson, D. J. Singh, and C. Fiolhais, Phys. Rev. B **46**, 6671 (1992).